Recent Developments in Top-Emitting Organic Light-Emitting Diodes

ARTICLE *in* ADVANCED MATERIALS · DECEMBER 2010

Impact Factor: 17.49 · DOI: 10.1002/adma.201001167 · Source: PubMed

7 AUTHORS, INCLUDING:

Shufen Chen
Nanjing University of Posts and Telecomm…
61 PUBLICATIONS **587** CITATIONS
SEE PROFILE

Ling-Hai Xie
Nanjing University of Posts and Telecomm…
149 PUBLICATIONS **1,972** CITATIONS
SEE PROFILE

Quli Fan
Nanjing University of Posts and Telecomm…
97 PUBLICATIONS **1,386** CITATIONS
SEE PROFILE

Wei Huang
University of Hawai'i at Mānoa
1,359 PUBLICATIONS **30,637** CITATIONS
SEE PROFILE

Recent Developments in Top-Emitting Organic Light-Emitting Diodes

By *Shufen Chen, Lingling Deng, Jun Xie, Ling Peng, Linghai Xie, Quli Fan,* and *Wei Huang**

Organic light-emitting diodes (OLEDs) have rapidly progressed in recent years due to their unique characteristics and potential applications in flat panel displays. Significant advancements in top-emitting OLEDs have driven the development of large-size screens and microdisplays with high resolution and large aperture ratio. After a brief introduction to the architecture and types of top-emitting OLEDs, the microcavity theory typically used in top-emitting OLEDs is described in detail here. Then, methods for producing and understanding monochromatic (red, green, and blue) and white top-emitting OLEDs are summarized and discussed. Finally, the status of display development based on top-emitting OLEDs is briefly addressed.

1. Introduction

The phenomenon called electroluminescence was first observed in single anthracene in 1965.[1] It remained merely an academic interest for the next two decades because a very high voltage (≈1000 V) was required to produce luminance and difficulties were associated with obtaining single crystals and forming nanometer-sized thin films. In 1987, Tang and Vanslyke[2] at Eastman Kodak reported the development of a two-layer organic structure made by vacuum deposition, which had high luminous efficiency and required a low driving voltage. In 1990, Burroughes et al.[3] first reported polymer light-emitting devices based on the conjugated polymer poly(*p*-phenylene vinylene). Since then, organic light-emitting diodes (OLEDs) have attracted the attention of many researchers. Developments have rapidly progressed in recent years because of the many important advantages that OLEDs present for displays, especially for flat panel displays (FPD). These advantages include highly luminous efficiency, wide viewing angle, low operating voltages, high brightness, vivid color, low cost, light weight, and particular flexibility. More than 100 academic communities (e.g., Princeton University, University of California at Santa Barbara, Technische Universität Dresden, Yamagata University, City University of Hong Kong, National Chiao Tung University, etc.) and corporations (e.g., Sony, Samsung, Pioneer, Kodak, eMagin, OSRAM, Merck, BASF, etc.) are investigating and developing OLEDs or high performance materials. Small- and middle-sized FPDs based on OLEDs have also been widely displayed in the market.

In general, an OLED has a multilayer structure, including an anode, a hole injection layer (HIL), a hole transporting layer (HTL), an electron blocking layer (EBL), an emitting layer (EML), a hole blocking layer (HBL), an electron transporting layer (ETL), an electron injection layer (EIL), and a cathode. In the devices reviewed here, the HIL and HTL are used to improve the injected hole numbers from the anode, which can be replaced by one layer possessing both hole injection and transporting abilities. Similarly, the EIL and ETL are used to enhance the injected electron numbers from the cathode and can also be replaced by one layer with both electron injection and transporting abilities. The EML is the location for hole and electron carrier recombination and can be one or several layers that recombine carriers with different band gaps (different colors). The HBL and EBL are beneficial because that they confine most of the carriers to the EML and enhance the luminous efficiency of the OLED.

OLEDs can be configured as top-emitting (or upwards-emitting) (**Figure 1b**), giving off light through a transparent or semitransparent top electrode, or bottom-emitting (or downwards-emitting) (Figure 1a), giving off light through a transparent bottom electrode and the substrate. Generally, the OLED display can be driven either by a passive matrix (PM) or an active matrix (AM) circuit, the difference between the two being the presence or absence of pixel driving circuits for each pixel. Although more difficult to fabricate, the AMOLED display has many advantages, such as high resolution, fast response, low power consumption, and large display area. To obtain a constant and uniform drive current in AMOLEDs (OLEDs are current driven devices), pixel driving circuits commonly include four or more backplane thin film transistors (TFTs) in combination with one capacitor.[4,5] However, a large number of TFTs fabricated on the substrate will invariably reduce the aperture ratio (AR) (Figure 1c) of each pixel of a bottom-emitting OLED (BEOLED). The reduced aperture ratio, in turn, requires a much higher driving current density to achieve the same level of luminance for display with pixels of larger AR.[6,7] Fortunately, top-emitting OLEDs (TEOLEDs,[8–10] Figure 1d) are structurally unaffected by

[*] Dr. S. Chen, Dr. L. Deng, J. Xie, Dr. L. Peng, Dr. L. Xie, Prof. Q. Fan, Prof. W. Huang
Key Laboratory for Organic Electronics and Information Displays (KLOEID) and Institute of Advanced Materials (IAM)
Nanjing University of Posts and Telecommunications (NUPT)
Nanjing 210046 (P. R. China)
E-mail: wei-huang@njupt.edu.cn

DOI: 10.1002/adma.201001167

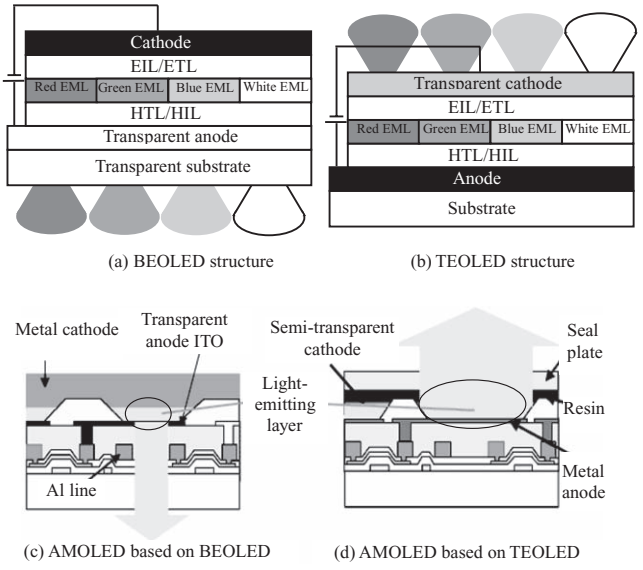

Figure 1. a) Bottom-emitting and b) top-emitting OLED structures; c,d) Schematic diagrams based on bottom-emitting and top-emitting OLEDs with low and high contrast ratio, respectively.

the number of TFTs integrated on the substrate because light emits from the top and, therefore, the OLED structure may be deposited on an opaque substrate (e.g., silicon), which makes it possible to hide the TFTs below the reflective anode. As a result, the AR of TEOLEDs can be greatly increased and the operating voltage is reduced for a given luminance, which could ultimately result in longer operational lifetime of devices.[11]

Similar to TEOLEDs, the so-called "inverted OLEDs" are also classified as surface- or top-emission structures. The only structural difference is that inverted OLEDs use the reflective bottom electrode as the cathode and the top (semi-)transparent anode is the side where light escapes. This is completely different from the bottom anode and the top (semi-)transparent cathodes in TEOLEDs. In addition, this structural difference between inverted OLEDs and TEOLEDs highlights an obvious difference in the driving pixel circuits of AMOLEDs. An inverted OLED is electrically connected to the drain of an n-type transistor with its cathode, while a TEOLED is connected to the drain of a p-type transistor with its anode (**Figure 2**). In general, electrical

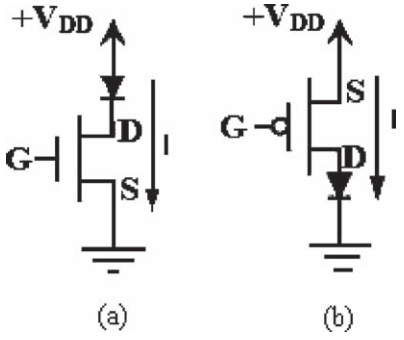

Figure 2. Cross-section of an AMOLED with a) an n-type driving transistor connected to an inverted OLED and b) a p-type driving transistor connected to a TEOLED.

Shufen Chen received her B.S., M.S., and Ph.D. degrees in Electronics from Jilin University in 2002, 2004, and 2007, respectively. She is working at the Institute of Advanced Materials at Nanjing University of Posts and Telecommunications. Her research interests include organic light-emitting diodes and organic solar cells.

Wei Huang received his B.S., M.S., and Ph.D. degrees in Chemical Physics from Peking University in 1979, 1982, and 1992, respectively. In 1993, he began his post-doctoral research in National University of Singapore, where he participated in the founding of Institute of Materials Research and Engineering. In 2001, he became a professor at Fudan University, where he founded and chaired the Institute of Advanced Material and Technology. In 2006, he was appointed vice president of Nanjing University of Posts and Telecommunications. His research interests include organic/plastic materials and devices and nano materials.

and optical characteristics in inverted OLEDs degrade due to changes in the formation process of the contact.[12–18] Thus, the major challenge for inverted OLEDs is to fabricate a high-performance device structures and to investigate the factors and mechanisms that affect electrical and optical characteristics.

In this paper, the development and progress of TEOLED technology (not including inverted OLEDs) in recent years is reported. A detailed discussion of different types of TEOLEDs and an introduction to the theory and methods to realize monochromatic and white light TEOLEDs are also included. In Section 2, all types of TEOLEDs are introduced, with consideration for emission colors and transparent cathode materials. In Section 3, the commonly used, basic microcavity theory is reported. In Section 4, the methods to realize monochromatic (red, green, and blue) and white light TEOLEDs are presented in detail. In the final section, the development, application, and prospects for TEOLEDs on FPDs are presented.

2. Types of TEOLEDs

2.1. TEOLEDs with Different Emission Colors

Any color can be obtained by the combination of the three basic colors, red (R), green (G), and blue (B). Red, green, and blue

emissions can be obtained from white light using color filters. Thus, up to now, both single color (R, G, and B) and white light are considered the most important emissions for application to full color displays and white light illumination and have therefore been widely researched in the OLED field. Red, green, blue, and white TEOLEDs with perfect performance characterized by high brightness, large luminous efficiency, low driving voltage, stable viewing angle, etc., are the major goals and have been investigated by scholars throughout the world in recent years. Design methods and corresponding reports about monochromatic and white color TEOLEDs will be discussed in detail in Section 4.

2.2. TEOLEDs with Different Cathodes

Two types of TEOLEDs, those based on metal oxides (transparent conducting oxides, TCOs) and those with metals as the cathode, have been developed in the last decade. The major difference between them is that the former has a high cathode transparency, while the latter has a relatively low light transmittivity (T). In other words, the cathodes made from metal oxides, such as indium tin oxide (ITO), indium zinc oxide (IZO), and indium oxide (IO), are transparent in the visible wavelength region, with T much larger than 80%, and those made from metals, such as Mg:Ag, Ag, Sm, Al, etc., are semitransparent, with T values often less than 70%.

Transparent conducting oxides, ITO,[19–21] IZO,[22,23] or IO,[24] are usually deposited using the direct current magnetron sputtering method, the radio frequency magnetron sputtering method, or ion beam assisted deposition. During conventional sputter deposition processing, energetic particles, such as reflected neutrons, high energy γ electrons, and charged ions, attack the surface of organic layers and transfer their high energies to the organic layers,[25] resulting in the degradation of the underlying organic layers. To reduce damage during the deposition of transparent conducting oxides layers, transparent or semi-transparent conducting buffer layers, such as MgAg,[8,23,26] CuPc,[9] Li or Al/CuPc and/or Al,[19,27] Li doped BCP[28] or BPhen,[29] Ca and/or LiF/Al,[21] Al and/or Ag,[21,24] 3,4,9,10-perlyenetetracarboxylic dianhydride (PTCDA),[9] metal acetylacetonate complexes $Ni(acac)_2$, $Mg(acac)_2$, $Ca(acac)_2$,[30] or pentacene[17] are generally deposited on the device before the deposition of the TCO layer. Even though the addition of such buffer layers may reduce energetic plasma damage during the TCO deposition, completely avoiding plasma damage is not easy because of the high sensitivity of organic films to radiation, charging, and heating. In 2006, Kim et al.[23] reported a plasma-damage-free sputtering method for the IZO cathode layer, which uses the box cathode sputtering technique. Using this approach, they obtained a TEOLED with a very low leakage current density of 1×10^{-5} mA cm^{-2} at a reverse bias of −6 V. The introduction of the additive buffer layers also led to a decrease in the T value of the cathode.

Entirely different from the TCO cathode, the use of a metal cathode in TEOLEDs can almost completely avoid the damage to the underlying organic layers because of the thermal evaporation technology available and the relatively low deposition temperatures required. As a result, more people would like to utilize metals (e.g., Al and/or Ag;[31–48] Ca;[49,50] Ca/Mg;[50–52] Ca/Ag;[11,53–59] Mg:Ag;[60,61] Sm[62], Sm/Ag, or Sm/Au;[63–67] Yb/Au or Ag;[68–70] Au;[49] and Al/SiO:Al[71]) as the TEOLED cathode, even though the T of even thin metal layers is much lower than that of TCO. Furthermore, the effects from the microcavities that exist in TEOLEDs influence certain emission characteristics, such as the emissive wavelength, the electroluminescent (EL) spectra, and the viewing angle. Naturally, attempts have been made to reduce microcavity effects by using light outcoupling layers, such as tris-(8-hydroxyquinoline) aluminum (Alq_3),[31,34,44,58,63] TeO_2,[33,35,52] ZnSe,[50,51] N′,N′-tetrakis(4-methoxyphenyl)-benzidine (MeO-TPD),[41,42,45] poly(9,9-dioctylfluorene-co-benzothiadiazole) (F8BT),[43] and 2,9-dimethyl-4,7-diphenyl-1, 10-phenanthroline (BCP).[65–67]

3. Microcavity Theory

Although a high T occurs in a TCO cathode, most buffer layers placed under the TCO can reduce the T of the cathode. Microcavity effects also occur in these devices, similar to those that occur when metals are used as cathodes.

3.1. Fabry-Pérot Cavity

A planar microcavity structure consists of a reflective anode, a semi-transparent cathode, and organic layers sandwiched in between (**Figure 3**). The anode and the cathode are parallel mirrors and they form a Fabry-Pérot resonator, which satisfies the following equation[72]:

$$\frac{2\pi}{\lambda}\sum_{m} 2n_m d_m \cos\theta_0 - \Phi_1(\lambda) - \Phi_2(\lambda) = k2\pi \quad (1)$$

where λ is the resonant wavelength or the peak wavelength; n_m and d_m are the refractive index and the thickness of the mth organic layer inside the two electrodes (the absorption of organic materials is neglected); θ_0 is the internal observation angle from the surface normal of the microcavity; $\Phi_1(\lambda)$ and $\Phi_2(\lambda)$ are the phase changes upon reflection corresponding to the effective reflectivities of R_1 and R_2 at the interfaces of the opaque anode/organic material and the organic material/semi-transparent cathode, respectively; and k is the mode number. When the electrodes are metals, $\Phi_1(\lambda)$ and $\Phi_2(\lambda)$ can be expressed with Equations (2) and (3)[73]:

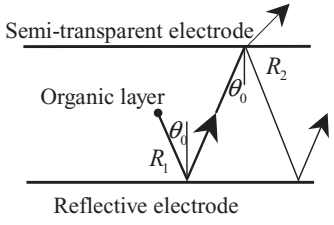

Figure 3. Fabry-Pérot cavity structure.

$$\Phi_{1,2}(\lambda) = \arctan\left(\frac{2n_0 B\cos\theta_0}{n_0^2\cos^2\theta_0 - A^2 - B^2}\right) \quad (2)$$

and

$$\Phi_{1,2}(\lambda) = \arctan\left[\frac{2n_0\cos\theta_0\left[2N_m K_m A - B(N_m^2 - K_m^2)\right]}{n_0^2(A^2 + B^2) - \cos^2\theta_0(N_m^2 + K_m^2)^2}\right] \quad (3)$$

(for P polarization)

For the electrode constructed with a dielectric quarter-wave stack, the phase change $\Phi_2(\lambda)$ can be described with $2\pi(n_{aver}/\Delta n)$.[74] Here, Δn and n_{aver} are the difference between and the average of the refractive indices of the two dielectric materials, respectively. The incident angle, θ_0, and polarization are considered in Equation (2) and (3) because the phase changes for *P*- and *S*-polarization are completely different when θ_0 deviates from 0 degrees. The phase changes originate from the calculation of the reflectivity of the electrodes.

For *P*-polarization,[73]

$$\eta_P = N/\cos\theta \quad (4)$$

$$R_P = \left(|r_P| e^{j\Phi_P}\right)^2 = \left(\frac{\eta_{0P} - \eta_{1P}}{\eta_{0P} + \eta_{1P}}\right)^2 = \left(\frac{n_0\cos\theta_1 - N_1\cos\theta_0}{n_0\cos\theta_1 + N_1\cos\theta_0}\right)^2 \quad (5)$$

For *S*-polarization,[73]

$$\eta_S = N\cos\theta \quad (6)$$

$$R_S = \left(|r_S| e^{j\Phi_S}\right)^2 = \left(\frac{\eta_{0S} - \eta_{1S}}{\eta_{0S} + \eta_{1S}}\right)^2 = \left(\frac{n_0\cos\theta_0 - N_1\cos\theta_1}{n_0\cos\theta_0 + N_1\cos\theta_1}\right)^2 \quad (7)$$

In these equations, r_P and r_S are the complex Fresnel coefficients for reflection of a wave, corresponding to *P*- and *S*-polarizations; R_P and R_S are the energy reflection coefficients or the so-called reflectivities for *P*- and *S*-polarization; n_0 and N_1 denote the refractive indices of the organic layer adjacent to the electrode and the electrode, where $N_1 = N_m - jK_m$ is the complex refractive index and $N_1\cos\theta_1 = A - jB$; and θ_0 and θ_1 are input and output angles in the organic and metal layers.

3.2. EL Spectra

The approximate theoretical spectrum for normal emissions in relation to the plane of the device layers was calculated following the approach of Deppe et al.[38,40,46,74–77] The theoretical EL spectrum is expressed as

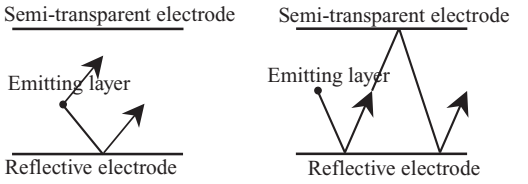

(a) Wide-angle interference (b) Multiple-beam interference

Figure 4. a) Wide-angle and b) multiple-beam interference in a cavity.

$$\left|E_{cav}(\lambda)\right|^2 = \frac{\frac{(1-R_2)}{i}\sum_i\left[1 + R_1 + 2\sqrt{R_1}\cos\left(\frac{4\pi z_i\cos\theta_0}{\lambda} + \Phi_1\right)\right]}{1 + R_1R_2 - 2\sqrt{R_1R_2}\cos\left(\frac{4\pi L\cos\theta_0}{\lambda} + \Phi_1 + \Phi_2\right)}\left|E_{nc}(\lambda)\right|^2 \quad (8)$$

where z_i is the optical thickness of the *i*th emitting dipole from the reflective metal mirror; $L = \sum_m n_m d_m$ is the total optical thickness between the two electrodes; and $|E_{nc}(\lambda)|^2$ is the free space EL intensity at λ. Equation (8) provides a qualitative understanding of the main effects produced by the microcavity.

3.3. Modulation Factors of Wide-Angle and Multiple-Beam Interferences

In a cavity device, both wide-angle and multiple-beam interference contribute to the EL spectra. **Figure 4a** shows that wide-angle interference is the interference between the directly emitted light and reflected light that have the same wave vector. The distance between the emission region and the reflective electrode plays an important role. Multiple-beam interference takes place when the radiation is reflected back and forth between the two electrodes (Figure 4b).

In Equation (8), the term $1 + R_1 + 2\sqrt{R_1}\cos(4\pi z_i\cos\theta_0/\lambda + \Phi_1)$ is only influenced by wide-angle interference, and thus, it is called the modulation factor of wide-angle interference[78]; meanwhile, the term $1 + R_1R_2 - 2\sqrt{R_1R_2}\cos(4\pi L\cos\theta_0/\lambda + \Phi_1 + \Phi_2)$ is called the modulation factor of multiple-beam interference.

3.4. Full Width at Half-Maximum

The full width at half-maximum (FWHM) can be estimated by[46,79,80]

$$FWHM = \frac{\lambda^2}{2L_{\text{eff}}}\times\frac{1 - \sqrt{R_1R_2}}{\pi\sqrt[4]{R_1R_2}} = \frac{\lambda^2}{2\left(\sum_m n_m d_m\cos\theta_0 + \frac{|\Phi_1(\lambda)|}{4\pi}\lambda + \frac{|\Phi_2(\lambda)|}{4\pi}\lambda\right)}\times\frac{1 - \sqrt{R_1R_2}}{\pi\sqrt[4]{R_1R_2}} \quad (9)$$

Spectral narrowing is the most common phenomenon caused by strong microcavity effects. As implied from Equation (9), the influence of the peak wavelength, λ, on the

FWHM is much stronger than that of the effective cavity, $L_{\text{eff}} = \sum_m n_m d_m \cos\theta_0 + |\Phi_1(\lambda)|\lambda/4\pi + |\Phi_2(\lambda)|\lambda/4\pi$.

3.5. Emission Enhancement Factor $G_{\text{cav}}(\lambda)$ and Integrated Enhancement Factor $G_{\text{int}}(\lambda)$

Microcavity effects inevitably exist in TEOLEDs fabricated with two high reflective electrodes, leading to redistributed photon densities of states, which give rise to sharper EL spectra and change the transition rates of the molecular excited states. The resonant emission enhancement factor, $G_{\text{cav}}(\lambda)$,[79–83] can be used to describe the magnified light from the cavity in the forward direction at the wavelength λ:

$$G_{\text{cav}}(\lambda) = \frac{\xi}{2}\frac{\left(1+\sqrt{R_1(\lambda)}\right)^2 \times \left(1-R_2(\lambda)\right)}{\left(1-\sqrt{R_1(\lambda)R_2(\lambda)}\right)^2}\frac{\tau_{\text{cav}}}{\tau} \quad (10)$$

In Equation (10), ξ is the antinode enhancement factor, which takes on the values 2 and 0 when the active region (exciton recombination zone) localizes at the antinode and the node of the standing wave, respectively; τ_{cav} and τ are lifetimes of the molecular excited state in the cavity and in the free space, respectively; $R_1(\lambda)$ is the reflectivity of the opaque anode; and $R_2(\lambda)$ and $T_2(\lambda) = 1 - R_2(\lambda)$ are the effective reflectivity and transmittivity of the cathode, respectively.

Emission enhancement factor, $G_{\text{cav}}(\lambda)$, is enhanced at the resonance wavelength, while off-resonance the emission is strongly suppressed. Thus, the spectrally integrated enhancement, $G_{\text{int}}(\lambda)$, defined as the integrated enhancement factor, is more important in the application of OLEDs:

$$G_{\text{int}} = \int S(\lambda)G_{\text{cav}}(\lambda)\mathrm{d}\lambda \Big/ \int S(\lambda)G_{\text{non}}(\lambda)\mathrm{d}\lambda \quad (11)$$

where $G_{\text{int}}(\lambda)$ is the integration only in the forward direction, $G_{\text{non}}(\lambda)$ is the emission enhancement of an optimized noncavity OLED (i.e., satisfying antinode and resonance conditions), and $S(\lambda)$ is an intrinsic emission spectrum.

The spatial distribution, which should also be considered when the total enhancement of cavity emission, is calculated by integrating over the solid angle as

$$G_{\text{tot}} = \int_\lambda \int_{2\pi} S(\lambda)G_{\text{cav}}(\lambda)\mathrm{d}\Omega\mathrm{d}\lambda \Big/ \int_\lambda \int_{2\pi} S(\lambda)G_{\text{non}}(\lambda)\mathrm{d}\Omega\mathrm{d}\lambda \quad (12)$$

4. TEOLEDs

Three types of TEOLEDs based on the three primary colors, R, G, and B, have been widely researched since 1994. Compared to BEOLEDs, the fabrication of TEOLEDs with perfect performance characterized by pure color and high efficiency requires a more complicated design of the cavity length or careful selection of semitransparent cathodes/outcoupling layers due to existence of microcavity effects.

In early research highly transparent metals were used as the semitransparent cathode. The microcavity effects in these devices are weak and the length in the cavity can be any value that does not satisfy the resonant modes. For metal cathodes with relatively low transmittance in the visible range, a light outcoupling layer can alter the distribution of the transmitted and reflected light, and, furthermore, a light outcoupling layer with the proper thickness enhances the transmitted intensity of the emission. Such a layer is deposited on the surface of the cathode. Some researchers paid much attention to a structure design in which the total organic thickness between the two reflective electrodes satisfies Equation (1). Using the microcavity to improve color purity and realize light magnification is seen as a favorable method.

4.1. Red and Green TEOLEDs

In 1994, Parker et al.[49] reported a single layer TEOLED based on the yellow emission of poly[2-methoxy, 5-(2′-ethyl-hexyloxy)-1,4-phenylene-vinylene] (MEH-PPV, **Figure 5a**). A highly transparent layer of Ca (20 nm) or Au (10 nm) was used as the cathode, and yellow emission from MEH-PPV was obtained because of the restrained microcavity effects, even though the thickness of the polymer layer was not designed and optimized using the theoretical equations. Similarly, Moon et al.[55,57,59] built multilayer devices based on the red emission of bis[2-(2′-benzothienyl)-pyridinato-N,C$^{3'}$]iridium(acetylacetonate) (BtpIr(acac), Figure 5b) with a highly transparent Ca (10 nm)/Ag (10 nm) layer for the cathode. They obtained red emission even though the physical cavity lengths of 95 and 110 nm did not satisfy the red emission resonant mode. Similarly, for green TEOLEDs, the design work of organic layer thickness can be neglected and green emission can be obtained from the devices when the cathode has a high transparency, as is the case for Ca (10 nm)/Ag (10 nm),[54] Ba (10 nm)/Ag (8 nm),[84] Yb:Au (or Ag) (19 nm),[69] etc.

Widely used metal cathodes like Al and Al/Ag have films with low transparency. Generally, two methods are used to obtain a pure red or green emission from TEOLEDs. The first method is to design the cavity length between the two reflective electrodes and make it match with the resonant mode of the red or green emission peak. The work mentioned in much of the literature[48,63,85] is of to this type. The cavity length that satisfies the red or green emission has a thickness similar to that usually used in BEOLEDs. Thus, the fabrication of red and green TEOLEDs, both with stable EL characteristics and low driving bias, is relatively easy. The second method is to fabricate red and green TEOLEDs by introducing an ITO anode with its thickness adjusted to fit the total optical length between the two reflective electrodes (**Figure 6**). In 1996, Grüner et al.[32] fabricated a TEOLED utilizing a distributed Bragg reflector (DBR) and Al as reflective mirrors. By controlling the thickness of the ITO anode and the single-layer organic PPV layer to be 75 nm and 75 nm ± 5 nm, respectively, a red EL emission was obtained even though the intrinsic color of PPV is green. The emissive material Alq_3 covered wide EL spectra with the peak wavelength of 528 nm. Han[71] and Cao[46] reported an Alq_3-based adjustable color emission from bluish green to red (500 to 680 nm) by merely changing the ITO film thickness between the two reflective layers. Using the same method, Hsu[11] and Cao[46] also accurately calculated the cavity lengths corresponding to

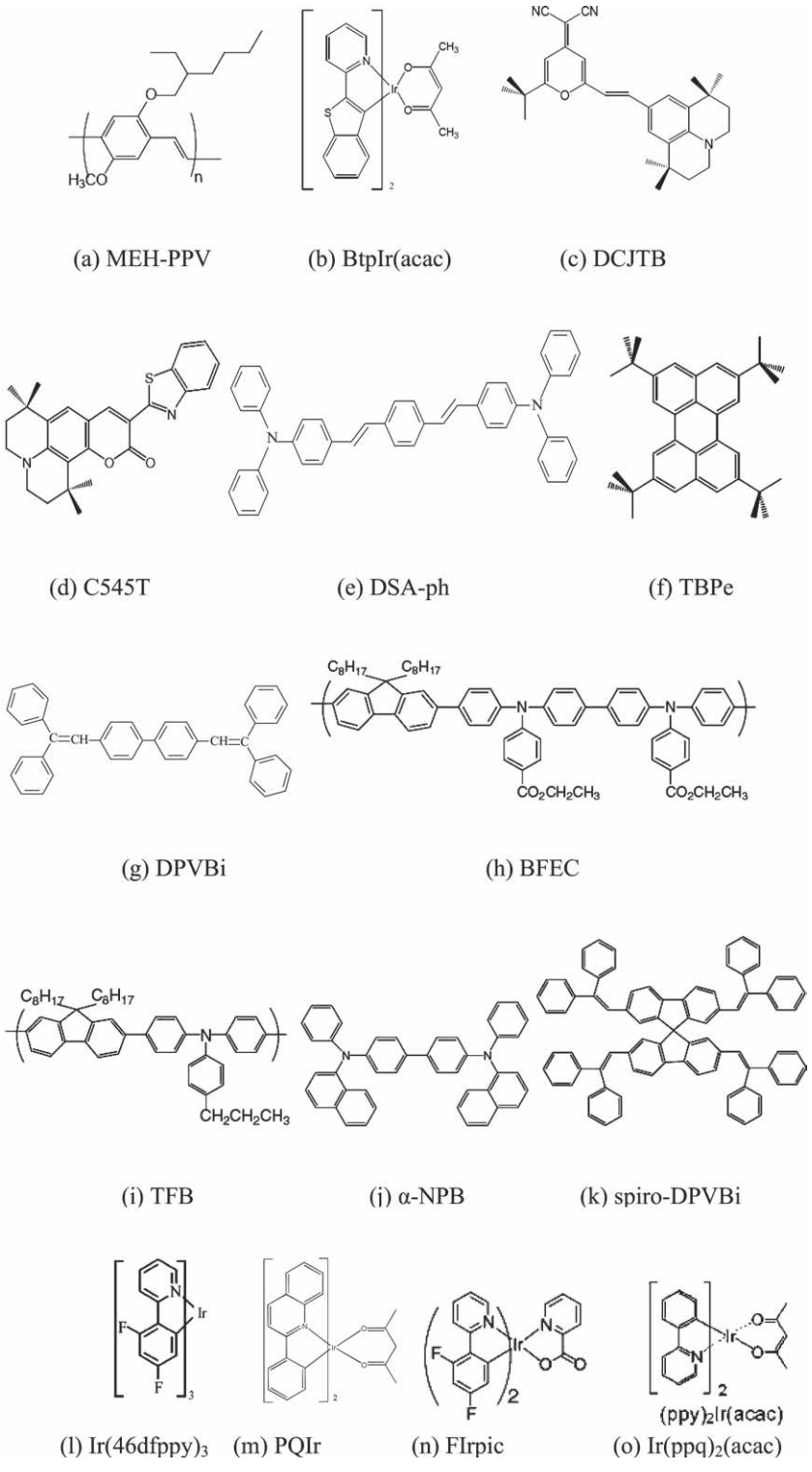

Figure 5. Molecular structures.

red, green, and blue emissions and adjusted the ITO anode thickness to satisfy the resonant wavelength of red emission from 2-{2-(*t*-butyl)-6-[(*E*)-2-(1,1,7,7-tetramethyl-2,3,6,7-tetrahydro-1*H*,5*H*-pyrido[3,2,1-*ij*]quinoline-9-yl)-1-ethenyl]-4*H*-4-pyranliden}malonitrile (DCJTB, Figure 5c), green emission from 10-(1,3-benzothiazol-2-yl)-1,1,7,7-tetramethyl-2,3,6,7-tetrahydro-1*H*,5*H*,11*H*-pyrano[2,3-*f*]pyrido[3,2,1-*ij*]quinoline-11-one (C545T, Figure 5d), and blue emission from *p*-bis(*p*-*N*,*N*-diphenylaminostyryl)benzene (DSA-ph, Figure 5e) or 2,5,8,11-tetra-butylperylene (TBPe, Figure 5f). With this method, highly saturated red, green, and blue emissions can be achieved.

4.2. Blue TEOLEDs

Microcavities with different cavity lengths can effectively modulate the peak wavelength and purify the emission color. Generally speaking, the cavity length (0 mode) that corresponds to red or green emission is typically used for the organic layer thickness. It has advantages such as low turn-on voltage and stable luminance under a driven bias of 5–15 V. However, the major peak wavelength of blue emission is much shorter than those of red and green emissions. That means a much shorter (0 mode) or longer (1, 2, and higher modes) cavity length for blue TEOLEDs, according to Equation (1). For example, the organic layer thicknesses that correspond to the resonant wavelength of the blue emission material 4,4′-bis(2,2′-diphenylvinyl)-1,1′-biphenyl (DPVBi, 464 nm peak, Figure 5g), with a device structure of Ag (100 nm)/4,4′-bis[N-(1-naphthyl-1-)-N-phenyl-amino]-biphenyl (NPB)/DPVBi/Alq_3/LiF(1 nm)/Al (1 nm)/Ag (20 nm) are 73, 205, and 337 nm for 0, 1, and 2 modes, where the thin layers of LiF and Al are neglected and all refractive indices of the organic layers are approximately 1.76 at 464 nm. The thickness of 73 nm for 0 mode is too thin to obtain a stable EL with a relatively high brightness. Moreover, the thicknesses of 205 and 337 nm for 1 or 2 modes are too thick to obtain a low turn-on voltage and high luminance under a commonly driven bias of less than 10 V.

To acquire blue emission with the driving voltage similar to those for red or green emission, several methods, such as a thickness-adjustable transparent electrodes (ITO) or HTLs, light outcoupling layers, tunable optical films (TOFs), and phase-shift adjustment layers, are used to design the device structure, which is discussed in detail below.

4.2.1. Thickness-Adjustable Transparent Electrodes

An effective method to obtain a blue emission from microcavitiesis to insert a transparent electrode (e.g., ITO) into the

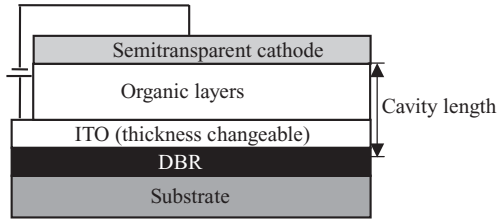

Figure 6. Microcavity structure with a DBR and a semitransparent metal as reflective electrodes. The cavity length can be changed by altering the ITO thickness.

reflective layer and HTL, similar to the configuration in Figure 6, with DBR replaced by a reflective metal such as Ag, where ITO is the anode and the thickness is adjustable. Due to high transparency and fine electric conductivity of ITO, no additional emission is adsorbed in this layer and the driving voltage is not enhanced. This type of work may be found in the literature.[11,46,56]

With this method, a highly saturated blue light emits with the Commission International de l'Eclairage (CIE, 1931) color coordinates near the standard blue emission of (0.14, 0.08). The disadvantage of this method is a relatively low emission efficiency due to the intrinsically broad EL spectra of the blue emitter and a complicated technological flow when applied in full-color OLED displays.

4.2.2. Varying HTL Thickness

In 2007, Chin et al.[61] reported R, G, and B TEOLEDs with thick hole transport layers of BFEC (or TFB)/α-NPB. Here, BFEC, TFB, and α-NPB are the abbreviations for poly(9,9′-dioctylfluorene-co-bis-N,N′-(4-ethoxycarbonylphenyl)-bis-N,N′-phenyl-benzidine, poly(9,9′-dioctylfluorene-co-N-(4-butylphenyl) diphenylamine), and N,N′-diphenyl-N,N′-bis(1-naphthyl)-(1,1′-biphenyl)-4,4′-diamine, respectively. The molecular structures are shown in Figure 5h–j. By optimizing the thickness of BFEC (or TFB)/α-NPB to 0/90 and 20/70 nm, the luminous efficiency of 1.4–1.89 cd A^{-1} and the CIE color coordinates of (0.13–0.14, 0.05–0.06) are obtained from the blue material 2,2′,7,7′-tetrakis-(2,2′-Diphenylvinyl)-spiro-9,9′-bifluorene (spiro-DPVBi) (Figure 5k), which gives pure blue emission and has good EL performance. The realization of R, G, and B TEOLEDs with good EL performance, including a relatively low turn-on voltage of 3.2–3.7 V, is mainly due to the relatively high mobility of α-NPB, which has a hole mobility of 3×10^{-4} cm^2 $V^{-1}s^{-1}$.

Although the resulting top-emitting devices exhibit appropriate color purity and efficiency, further improvements, particularly in the intrinsic mobility of the transport materials, are required to fabricate more efficient and low driving voltage TEOLEDs based on thicker transport layers.

4.2.3. Light Outcoupling Layers

Another important method by which to obtain blue top emission is to utilize a light outcoupling layer with proper physical thickness, with which the R of the cathode (including the light outcoupling layer) can be reduced to a minimum value at the blue-emission peak wavelength. Furthermore, the microcavity effects in these devices can be restrained and the intrinsic blue light can be emitted from the top-emitting device.[45,67] For example, Chen et al.[67] employed a BCP light outcoupling layer to enhance T and reduce R with a Sm (11 nm)/Ag (12 nm) cathode (**Figure 7**). By optimizing the BCP layer to 35 nm, the maximum T value increases to 59.4%, while R decreases to 6.7% around the emissive peak of DPVBi (464 nm). Here, the microcavity effect caused by multiple-beam interference (Figure 4b) is expected to be as weak as possible and blue light emits easily from the TEOLED. The CIE coordinates of the blue emission change from (0.201, 0.263) to (0.173, 0.199) when the bias is varied from 6 to 17 V, which are similar to the chromaticity coordinates of (0.16, 0.16) for the BEOLED.[86] In addition, a weak multiple-beam interference in the BCP-covered TEOLED brings stable EL spectra from 0 to 75° (**Figure 8**), which is very necessary and helpful in the build-up of OLED displays.

With this approach, a main advantage is that any thickness can be used for the total organic layers (e.g., a widely used value is 100 nm[67]), without the influence of microcavity. This method can also be applied to the fabrication of red and green TEOLEDs. When this method is applied to construct full color displays, the fabrication process can be simplified by avoiding the complicated ITO masking process before the deposition of organic materials, since the ITO thickness must be adjusted to obtain a different resonant cavity for RGB colors.

Based on reference,[67] Chen et al.[87] introduced a new way to enhance the EL intensity of blue top emission, where wide-angle interference is used in the design of the device structures. By optimizing the layer thickness between the reflective anode and the emissive layer, enhancement of the interference between the reflective light and the intrinsic blue light can be realized. This method is also suitable for the design of red and green top-emissive devices.

4.2.4. TOFs

Hou et al.[88] first used TOFs on a semitransparent cathode to realize RGB primary colors, in which case the TOFs were

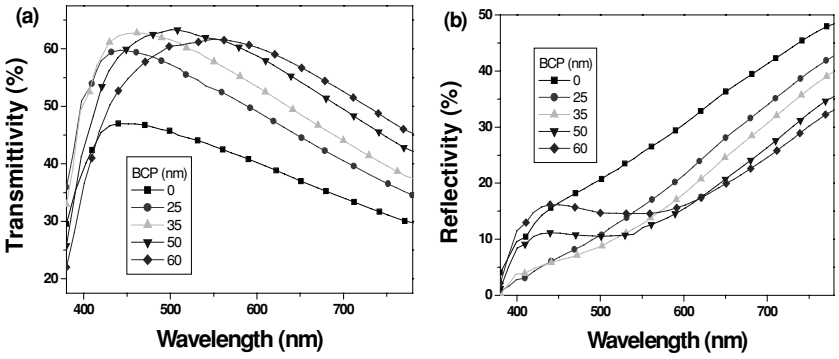

Figure 7. a) Transmittivity and b) reflectivity characteristics of the DPVBi (30 nm)/Alq_3 (20 nm)/Sm (11 nm)/Ag (12 nm)/BCP/air multilayer system. Here, the thickness of the BCP layer is varied from 0 nm to 60 nm. Reproduced with permission.[67] Copyright 2008, Elsevier.

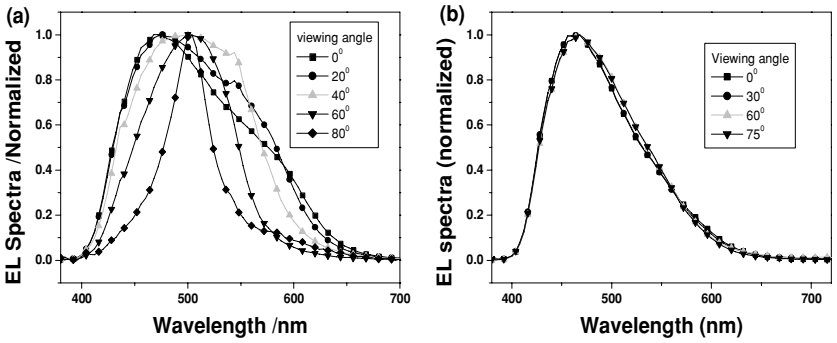

Figure 8. EL spectra changes of blue TEOLEDs with the viewing angle a) without and b) with the BCP outcoupling layer. Reproduced with permission.[67] Copyright 2008, Elsevier.

constructed with an organic Alq_3 layer and a 20-nm-thin Ag layer on one side and a 20 nm semitransparent Ag cathode on the other side. **Figure 9** shows the schematic structures of the OLEDs with and without TOFs. By changing the thickness of Alq_3 to x = 60, 90, and 120 nm, the transmittance of the trilayer structure Ag (20 nm)/Alq_3 (x nm)/Ag (20 nm) has a maximum value at the B, G, and R emission peaks, respectively (**Figure 10**). Based on both a single color with wide spectra or a white emission (white TEOLED structure: Glass/Al 10 nm/Ag 80 nm/V_2O_5 7 nm/PEDOT:PSS 40 nm/mCP:10 wt% FIrpic:1 wt% $Ir(ppq)_2(acac)$ 40 nm/BCP 10 nm/Alq_3 20 nm/Sm 10 nm/Ag 20 nm) and the corresponding transparency in the B, G, and R regions, the desired B, G, and R emissions are obtained (**Figure 11**). Here, PEDOT:PSS, mCP, FIrpic, $Ir(ppq)_2(acac)$ are the abbreviations of poly(ethylenedioxythiophene):poly(styrene sulfonic acid), 1,3-bis(9-carbazolyl)benzene, iridium (III) bis[(4,6-di-fluoropheny)-pyridinato-N,C^2]picolinate, and bis(2,4-diphenyl-quinoline)iridium(III) acetylan-etonate-, respectively. The emission peaks of B, G, and R at 470, 520, and 620 nm correspond to the CIE coordinates (0.17, 0.25), (0.22, 0.51), and (0.62, 0.35), respectively. The efficiencies of B, G, and R are a somewhat low, with values of 0.3, 1.0, and 0.5 cd A^{-1}, respectively, because the light-emitting efficiency of the white TEOLED is only about 1.95 cd A^{-1}.

4.2.5. Phase-Shift Adjustment Layers (PSALs)

In 2009, Meng et al.[89] brought the phase shift, which is caused by the deposition of a light outcoupling layer onto the semitransparent cathode, into the design of a blue top-emission device. The phase shift is maximized by a particular thickness of the light outcoupling layer. Blue emission is acquired along with the recombination of the maximum phase shift and a proper cavity length (**Table 1**).

The shortcoming of this method is that the range of the phase shift is finite. For example, the maximum shift of the peak wavelength is 20 nm for the cavity length of 90 or 100 nm, while the maximum shift is 12 nm for the cavity length of 80 nm. Thus, the total organic thickness must be reduced to obtain a saturated color purity of blue light. For example, the recombination of an 80-nm-thick cavity length and a 50–70 nm Alq_3 phase shift layer can achieve a pure blue emission with a peak wavelength of 456 nm. However, this will cause a stability problem in EL devices.

In their paper, Meng et al. report fabrication of blue TEOLEDs based on a 90-nm-thick cavity length. With various Alq_3 PSAL thicknesses, they obtained a maximum peak shift of 16 nm when the PSAL thickness was 60 nm (**Figure 12**). The theoretically simulated spectra calculated according to Equation (8), which agree well with the measured spectra, are also depicted in the figure. The corresponding CIE coordinates of TEOLEDs with 60 nm PSAL thickness are (x = 0.13, y = 0.15) at 8 V, which is better than (x = 0.16, y = 0.16) obtained with BEOLEDs. The luminous efficiency in TEOLEDs has a slight improvement of 0.4 cd A^{-1} compared with that in BEOLEDs, bringing its value to 3.4 cd A^{-1}.

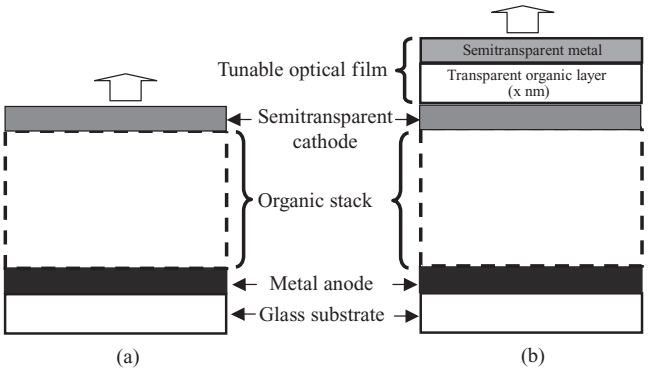

Figure 9. TEOLED a) without and b) with TOFs.

4.3. White TEOLEDs

White emission is commonly composed of the RGB or BY (Y: yellow) color mixture with emission spectra covering the broad

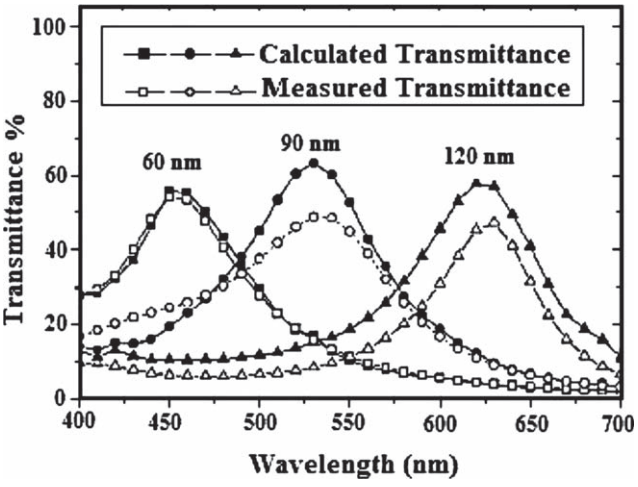

Figure 10. Calculated (closed symbols) and measured (open symbols) transmission spectra for Ag 20 nm/Alq_3x nm/Ag 20 nm with different thicknesses of the Alq_3 layer. Reproduced with permission.[88] Copyright 2008, Elsevier.

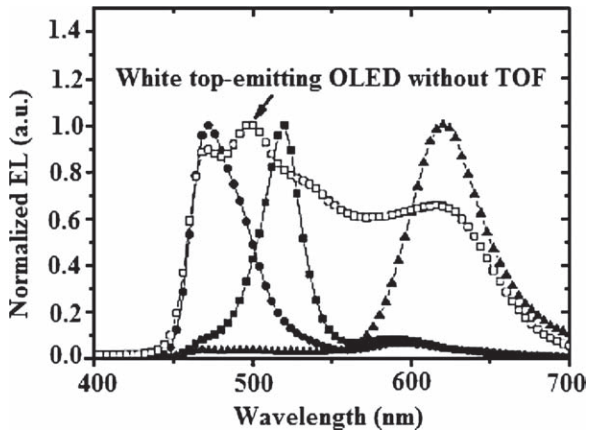

Figure 11. Normalized EL spectra of white TEOLEDs and color tunable TEOLEDs based on a white emissive organic stack at 10 V. Reproduced with permission.[88] Copyright 2008, Elsevier.

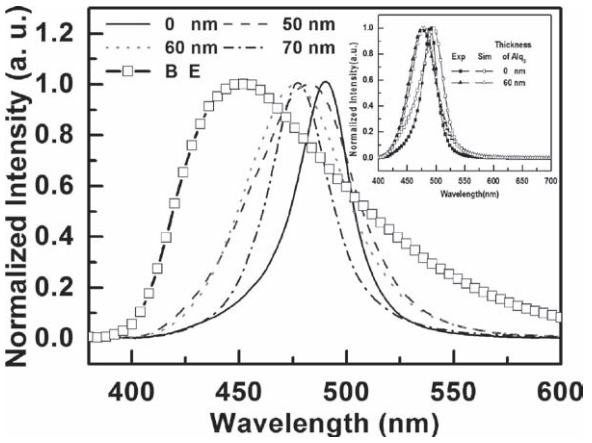

Figure 12. Experimental EL spectra of blue TEOLED capped by different PSALs (0, 50 nm, 60 nm, and 70 nm). BEOLED (open square) EL spectra are also depicted for comparison. Inset: Comparison of numerical simulation spectra and experimental EL spectra of blue TEOLED without and with 60-nm thick Alq_3. Reproduced with permission.[89] Copyright 2009, Optical Society of America.

range between 400 and 700 nm. Generally, in BEOLEDS, a white emission is easily obtained because of the high transparency of both the bottom anode ITO and the glass substrate. To obtain a white emission, researchers have employed various methods, such as one doped-emission layer or multilayer structures with RGB, BY, or RYGB colors;[90–97] excimer or exciplex emission;[98–103] microcavity structure with the resonant wavelengths at R, G, and B emission peaks;[76,104,105] blue emission with an incomplete energy down-conversion layer;[106] and tandem structure.[107] Unfortunately, although all of these methods suitably produce white light in BEOLEDs, they are not suitable for the construction of white TEOLEDs because of microcavity effects that exist in the TEOLEDs.

Considering the important influence of cathode transparency on the fabrication of white TEOLEDs, we discuss two types of devices that are used as cathodes: (1) highly transparent metal oxides like ITO and (2) semitransparent metals. Obtaining white top emission from TEOLEDs is easier with highly transparent metal oxides than with semitransparent metals.

4.3.1. ITO Transparent Cathode

In 2005, Kanno et al.[29] fabricated a white-emitting TEOLED based on the blue phosphor, tris-(1-(4,6-difluorophenyl)pyridinato, N, $C^{2'}$)iridium(III) ($Ir(46dfppy)_3$, Figure 5l), and the red phosphor, iridium(III) bis(2-phenyl quinolyl-N, $C^{2'}$)acetylacetonate (PQIr, Figure 5m). To obtain the white emission, highly transparent ITO is used as the cathode. With an effective Li-doped electron injection layer, the energy barrier from ITO cathode into the device is reduced and high external quantum and power efficiencies of 10.5% ± 1.0% (1.6 mA cm^{-2}) and 9.8 lm W^{-1} ± 1.0 lm W^{-1} (1.0 mA cm^{-2}) are achieved. The obtained CIE coordinates (x = 0.42, y = 0.39) are in the white light area.

Here, the ITO sputtering technology is crucial and at the same time hard to control; thus, more researchers would like to use metal films, instead of ITO, as the semitransparent cathodes by optimizing their thicknesses or introducing another light outcoupling layer. Optimizing thickness or introducing another light coupling layer effectively restrains microcavity effects and the deposition of commonly used metals, such as Ag, Al, Au, Sm, Yb, and Cu, causes almost no damage to the underlying organic layers.

4.3.2. Metal Semitransparent Cathodes

The key problem in building a white emission TEOLED addressed in this subsection is how to restrain microcavity effects caused by the reflective electrodes in order to obtain wide spectra in the visible range.

The first report on white emission TEOLED was authored by Tom Feng, a researcher at eMagin Corp., in 2001.[108] Feng employed a double-dopant structure to construct a white emission

Table 1. Simulated resonant wavelengths and maximum shifts associated with different thicknesses of PSALs and different cavity lengths. Reproduced with permission from [89]. Copyright 2009, Optical Society of America.

Cavity length [nm] [a]	Thicknesses of PSALs [nm]								Maximum shift [nm]
	0	10	30	50	60	70	90	100	
80	468	468	464	456	456	456	460	464	12
90	496	496	488	480	475	484	488	492	20
100	528	528	520	508	508	512	520	520	20

[a] Here the cavity length is the total thickness of organic layers sandwiched between two electrodes.

with relatively high luminous efficiencies of 4.9 cd A^{-1} and 1.9 lm W^{-1} at 20 mA cm^{-2} and 7.9 V. With the core white emission device structure, a SXGA resolution with 1280 × 1024 pixel format and black-and-white AMOLED microdisplay on silicon with an active viewing area of 15 × 12 mm^2 was realized. This was a trade secret so detailed information about the blue and red emissive materials and the cathode was not discussed.

Hou et al.[88] published a white emission structure with only one emissive layer containing the blue phosphor FIrpic (Figure 5n) and the red phosphor $Ir(ppq)_2(acac)$ (Figure 5o). They selected Sm (10 nm)/Ag (20 nm) as the semitransparent cathode and an 80-nm-thick Ag layer as the highly reflective anode. Then, a white emission with the EL spectra covering 450–650 nm and the CIE coordinates of ($x = 0.34$, $y = 0.41$) was obtained, but the light-emitting efficiency was merely about 1.95 cd A^{-1}. The low efficiency mainly resulted from microcavity effects (multiple-beam interference) caused by the relatively high reflection of the Sm(10 nm)/Ag (20 nm) cathode and high reflection of the Ag (80 nm) anode, leading to the restriction of a large part of the emissive wavelengths except those near the resonant wavelength. To obtain a white emission, the multiple-beam interference should be restrained by reducing the reflection of the electrodes.

In 2005, Hsu et al.[59] employed a SnO_2 index-matching layer on the Ca (5 nm)/Ag (15 nm) cathode. The transmittance of the CaAg cathode with the cover improved in the visible range between 450 and 650 nm and its optimization value reaches 80% when the SnO_2 thickness is 22.5 nm. Combining the highly transparent cathode with a calculated broad spectra FWHM from Equation (9) one obtains near-white light emission with the high EL efficiency of 22.2 cd A^{-1} and 9.6 lm W^{-1} at 20 mA cm^{-2} and 7.3 V and with CIE coordinates of (x = 0.31, y = 0.47). This is based on the blue emitting *p-bis*(*p-N, N-di*-phenyl-aminostyryl)benzene and yellow emitting rubrene. Under different viewing angles (0°, 30°, and 60°), the emission shows little angular dependence(**Figure 13**) and the three main peaks in the white emission remain the same when viewed at different angles.

In 2008, a white TEOLED with a long-life and a nearly Lambertian source was described.[109] The authors produced a white emission device with low-reflectivity molybdenum (Mo) anode ($R \approx 58\%$ in visible range) and an Al (1.5 nm)/Ag (17.5 nm) cathode together with a 30-nm-thick NPB capping layer to reduce cathode reflectivity. With the low reflectivity of both of the electrodes, the microcavity effect is effectively alleviated, a broad spectrum (FWHM = 160 nm) is obtained, and the emission spectrum is almost unchanged under different viewing angles. With a dual-layer emitter composed of doped blue (TC-1754) and yellow (TC-1776) dopant in the same blue host (TC-1556), a white emission with an EL efficiency of 3.7 cd A^{-1}, a low driving voltage of 4.9 V at 3000 cd m^{-2}, and CIE coordinates of ($x = 0.33$, $y = 0.39$), which are near the standard white light equal energy point ($x = 0.33$, $y = 0.33$), is obtained.

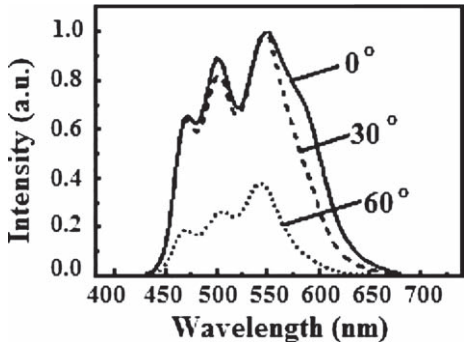

Figure 13. EL spectra of a white device under viewing angles of 0°, 30°, and 60° from the surface normal. Reproduced with permission.[59] Copyright 2005, American Institute of Physics.

Most reports about white emission TEOLEDs have a relatively low luminous efficiency when the semitransparent metal cathodes are used because the relatively strong microcavity effects restrain part of light emitted from the devices. Proper confinement of multiple-beam interference and employment of wide-angle interference may be beneficial to the enhancement of EL efficiency.

5. Applications and Developments

OLEDs emit their own light and have many appealing performance characteristics including: (1) lower power consumption, (2) high contrast, (3) a broader color gamut, (4) high-speed refresh rates, (5) a large viewing angle, (6) ease of view, (7) low cost systems solutions, (8) a wide operating temperature range, and (9) flexible and thin solid displays. Since the first commercial application in the panels of car radios by Pioneer in 1997, more than 100 corporations (including Sony, Sharp, Samsung, Philips, Pioneer, NEC, Kodak, Sanyo, LG, CDT, RiTDisplay, TDK, Univision, CMEL, eMagin, Intel, and Motorola) have devoted a huge amount of money and considerable manpower to design and take advantage of OLED display screens. With the exception of Sony and eMagin, most of these companies focus on the development of monochrome or full color display panels with BEOLED technology.

In 2001, Sony manufactured a 13-inch AMOLED display panel model using their "super top emission" technology. At the International Consumer Electronics Show (CES) 2007 in Las Vegas, they displayed a 27-inch large OLED TV working prototype[110] with 1920 × 1080 pixels and 200 cd m^{-2}. With super top emission technology, color filters, and microcavity interference effects, the OLED TV reached a high contrast of 1 000 000:1 and a wide color gamut over 100% NTSC standard. In the same year, they launched an 11-inch OLED TV named XEL-1, the first commercial, large-size OLED in the world. XEL-1 is an 11-inch display that is as thin as 3 mm and with a resolution of 1024 × 600 (**Figure 14**). However, due to expense and technical limitations (e.g., lifetime problems), no additional OLED TVs were released into the market in 2008 and 2009.

In recent years, Samsung has also used top-emission technology to take advantage of the small and middle-sized AMOLED display panel market.

eMagin is another company that is an early user of top-emission technology. It is the first and only manufacturer of AMOLED-on-silicon microdisplays. Organic light-emitting microdisplays can effectively incorporate the TEOLED structure on a silicon integrated circuit. Aside from this, microdisplays have advantages such as very low power consumption, high resolution, high contrast, high-speed refresh rates, compactness,

Figure 14. The first commercial, large-size XEL-1 OLED TV. Reproduced with permission from the Sony Corporation.

and portability. Microdisplay products have potential in markets for wearable computers, wireless communication appliances, portable entertainment, digital cameras, and many others. In 2001, eMagin used green and white OLED microdisplays with a pixel format of 1280 × 1024 and emission area of 15 mm × 12 mm to produce a device with total weight and OLED power consumption less than 10 g and 450 mW, respectively. Up to now, eMagin has taken advantage of the Super Video Graphics Array+ (SVGA+, 852 × 3 × 600)[111] and Super Extended Graphics Array (SXGA, 1280 × 3 × 1024)[111] series monochrome or full color OLED-XL microdisplay productions with 0.61- and 0.77-inch viewing areas and typical power consumption of less than 200 mW.

Flexibility is the most attractive factor for OLED application. In 2007, Sony announced the launch of a 2.5-inch flexible, color AMOLED with 120 × 160 pixels, and 8 gray levels. TEOLED structure and organic TFT were both adopted on this flexible AMOLED display. Mass production, however, has not yet been initiated by Sony.

In summary, although OLED (based on BEOLED or TEOLED) FPDs are unique and potentially superior to liquid crystal displays (LCDs), plasma display panels (PDPs), and cathode ray tubes (CRTs), problems such as lifetime and stable driving circuits are the stumbling blocks that have prevented OLED FPDs from being quickly released into the commercial market. As soon as these problems are resolved, we believe that OLED FPDs will become an important part of our lives, jobs, and even for our entertainment choices.

6. Conclusions

The most extensively used method for acquiring full-color OLED displays is to use RGB primary colors or white light with color filters, where the build-up of R, G, B, and white electroluminescence devices is critical.

In TEOLEDs, the microcavity effect commonly occurs, and when and how to restrain or make use of this effect is indispensable for device design. The microcavity theory presented in Section 3 of this article provides assistance for the construction of monochrome or white devices with high luminous efficiency and saturated color purity. Amongst all colors, blue top emission is the hardest to obtain. The most popular methods use the microcavity effect, which can satisfy the resonant peak of blue light by adjusting cavity length in ways such as using a thickness-adjustable transparent ITO electrode, using various hole-transporting layers, or employing tunable optical films placed onto the semitransparent cathode. Another aspect is to restrain microcavity resonance by introducing a light outcoupling layer onto the cathode, which is also usually employed during the fabrication of white TEOLEDs. In addition, a phase shift on the cathode caused by a light outcoupling layer, referred to as the phase-shift adjustment layer, was incorporated into the design of blue TEOLEDs.

Commercial progress toward top-emission-based OLED flat panel displays has been mainly promoted by Sony and eMagin. In recent years, some small and medium-sized OLED displays have been launched, but they have some technical shortcomings such as their lifetime, and the cost limits rapid development and application. We believe once these problems are resolved, all types of OLED products will become necessary parts of our daily lives.

Acknowledgements

The authors acknowledge financial support from the Ministry of Science and Technology (973 project, Grant No. 2009CB930600), National Natural Science Foundation of China (Grants No. 60907047, 20774043, 20704023, 60706017, 60977024, and 60876010), The Research Fund for the Doctoral Program of Higher Education (Grant No. 20093223120003), Natural Science Foundation of Jiangsu Province (Grants No. BK2009423 and BK2008053), and Natural Science Foundation of the Education Committee of Jiangsu Province (Grants No. 08KJB510013, 07KJB150082, SJ209003, TJ209035, and TJ207035).

Received: April 1, 2010
Published online: September 14, 2010

[1] W. Helfrich, W. G. Schneider, *Phys. Rev. Lett.* **1965**, *14*, 229.
[2] C. W. Tang, S. A. Vanslyke, *Appl. Phys. Lett.* **1987**, *51*, 913.
[3] J. H. Burroughes, D. D. C. Bradley, A. R. Brown, R. N. Marks, K. Mackay, R. H. Friend, P. L. Burns, A. B. Holmes, *Nature* **1990**, *347*, 539.
[4] J. H. Lee., W. J. Nam, S. M. Han, M. K. Han, *Dig. Tech. Pap. - Soc. Inf. Disp. Int. Symp.* **2003**, *34*, 490.
[5] J. C. Goh, C. K. Kim, J. Jang, *Dig. Tech. Pap. - Soc. Inf. Dsisp. Int. Symp.* **2003**, *34*, 494.
[6] Y. He, R. Hattori, J. Kanicki, *Jpn. J. Appl. Phys.* **2001**, *40*, 1199.
[7] C. Adachi, M. A. Baldo, S. R. Forrest, M. E. Thompson, *Appl. Phys. Lett.* **2000**, *77*, 904.
[8] V. Bulovic, G. Gu, P. E. Burrows, M. E. Thompson, S. R. Forrest, *Nature* **1996**, *380*, 29.
[9] G. Parthasarathy, P. E. Burrows, V. Khalfin, V. G. Kozlov, S. R. Forrest, *Appl. Phys. Lett.* **1998**, *72*, 2138.
[10] L. S. Hung, C. W. Tang, M. G. Mason, P. Raychaudhuri, J. Madathil, *Appl. Phys. Lett.* **2001**, *78*, 544.
[11] S. F. Hsu, C. C. Lee, S. W. Hwang, H. H. Chen, C. H. Chen, A. T. Hu, *Thin Solid Films* **2005**, *478*, 271.
[12] M. Pfeiffer, S. R. Forrest, X. Zhou, K. Leo, *Org. Electron.* **2003**, *4*, 21.
[13] V. Bulovi , P. Tian, P. E. Burrows, M. R. Gokhale, S. R. Forrest, M. E. Thompson, *Appl. Phys. Lett.* **1997**, *70*, 2954.

[14] C. W. Chen, C. L. Lin, C. C. Wu, *Appl. Phys. Lett.* **2004**, *85*, 2469.
[15] D. R. Baigent, R. N. Marks, N. C. Greenham, R. H. Friend, S. C. Moratti, A. B. Holmes, *Appl. Phys. Lett.* **1994**, *65*, 2636.
[16] T. Dobbertin, O. Werner, J. Meyer, A. Kammoun, D. Schneider, T. Riedl, E. Becker, H. H. Johannes, W. Kowalsky, *Appl. Phys. Lett.* **2003**, *83*, 5071.
[17] T. Dobbertin, M. Kroeger, D. Heithecker, D. Schneider, D. Metzdorf, H. Neuner, E. Becker, H. H. Johannes, W. Kowalsky, *Appl. Phys. Lett.* **2003**, *82*, 284.
[18] X. Zhou, M. Pfeiffer, J. S. Huang, J. Blochwitz-Nimoth, D. S. Qin, A. Werner, J. Drechsel, B. Maennig, K. Leo, *Appl. Phys. Lett.* **2002**, *81*, 922.
[19] H. W. Choi, S. Y. Kim, K. B. Kim, Y. H. Tak, J. L. Lee, *Appl. Phys. Lett.* **2005**, *86*, 12104.
[20] M. H. Lu, M. S. Weaver, T. X. Zhou, M. Rothman, R. C. Kwong, M. Hack, J. J. Brown, *Appl. Phys. Lett.* **2002**, *81*, 3921.
[21] L. H. Smith, J. Wasey, W. L. Barnes, *Appl. Phys. Lett.* **2004**, *84*, 2986.
[22] H. J. Shin, H. J. Song, J. Lee, H. J. Yoon, J. Chung, J. C. Lee, *J. Appl. Phys.* **2006**, *100*, 84504.
[23] H. K. Kim, K. S. Lee, J. H. Kwon, *Appl. Phys. Lett.* **2006**, *88*, 12103.
[24] J. T. Lim, C. H. Jeong, A. Vozny, J. H. Lee, M. S. Kim, G. Y. Yeom, *Surf. Coat. Technol.* **2007**, *201*, 5358.
[25] D. M. Mattox, *J. Vac. Sci. Technol.* **1989**, *A7*, 1105.
[26] G. Gu, V. Bulovi , P. E. Burrows, S. R. Forrest, M. E. Thompson, *Appl. Phys. Lett.* **1996**, *68*, 2606.
[27] L. S. Hung, C. W. Tang, *Appl. Phys. Lett.* **1999**, *74*, 3209.
[28] G. Parthasarathy, C. Adachi, P. E. Burrows, S. R. Forrest, *Appl. Phys. Lett.* **2000**, *76*, 2128.
[29] H. Kanno, Y. Sun, S. R. Forrest, *Appl. Phys. Lett.* **2005**, *86*, 263502.
[30] A. Yamamori, S. Hayashi, T. Koyama, Y. Taniguchi, *Appl. Phys. Lett.* **2001**, *78*, 3343.
[31] B. W. Xiao, B. Yao, C. S. Ma, S. Y. Liu, Z. Y. Xie, L. X. Wang, *Semicond. Sci. Tech.* **2005**, *20*, 952.
[32] J. Grüner, F. Cacialli, R. H. Friend, *J. Appl. Phys.* **1996**, *80*, 207.
[33] C. W. Chen, P. Y. Hsieh, H. H. Chiang, C. L. Lin, H. M. Wu, C. C. Wu, *Appl. Phys. Lett.* **2003**, *83*, 5127.
[34] Y. Q. Li, J. X. Tang, Z. Y. Xie, L. S. Hung, S. S. Lau, *Chem. Phys. Lett.* **2004**, *386*, 128.
[35] C. C. Wu, C. L. Lin, P. Y. Hsieh, H. H. Chiang, *Appl. Phys. Lett.* **2004**, *84*, 3966.
[36] C. J. Yang, C. L. Lin, C. C. Wu, Y. H. Yeh, C. C. Cheng, Y. H. Kuo, T. H. Chen, *Appl. Phys. Lett.* **2005**, *87*, 143507.
[37] W. F. Xie, Z. J. Wu, W. Hu, Y. Zhao, C. N. Li, S. Y. Liu, *Semicond. Sci. Tech.* **2005**, *20*, 443.
[38] S. J. Han, C. J. Huang, Z. H. Lu, *J. Appl. Phys.* **2005**, *97*, 93102.
[39] J. Feng, T. Okamoto, S. Kawata, *Appl. Phys. Lett.* **2005**, *87*, 241109.
[40] H. J. Peng, J. X. Sun, X. L. Zhu, X. M. Yu, M. Wong, H. S. Kwok, *Appl. Phys. Lett.* **2006**, *88*, 73517.
[41] Q. Huang, K. Walzer, M. Pfeiffer, K. Leo, M. Hofmann, T. Stubinger, *J. Appl. Phys.* **2006**, *100*, 64507.
[42] Q. Huang, K. Walzer, M. Pfeiffer, V. Lyssenko, G. F. He, K. Leo, *Appl. Phys. Lett.* **2006**, *88*, 113515.
[43] X. Y. Deng, M. K. Ho, K. Y. Wong, *J. Appl. Phys.* **2006**, *99*, 16103.
[44] J. Cao, X. Y. Jiang, Z. L. Zhang, *Appl. Phys. Lett.* **2006**, *89*, 252108.
[45] Q. Huang, S. Reineke, K. Walzer, M. Pfeiffer, K. Leo, *Appl. Phys. Lett.* **2006**, *89*, 26 3512.
[46] J. Cao, X. Liu, M. A. Khan, W. Q. Zhu, X. Y. Jiang, Z. L. Zhang, S. H. Xu, *Curr. Appl. Phys.* **2007**, *7*, 300.
[47] D. Hill, K. Leo, G. F. He, Q. Huang, *Appl. Phys. Lett.* **2007**, *90*, 101111.
[48] S. F. Chen, X. Li, W. F. Xie, Y. Zhao, C. A. Li, S. Y. Liu, *Thin Solid Films* **2008**, *516*, 3364.
[49] I. D. Parker, H. H. Kim, *Appl. Phys. Lett.* **1994**, *64*, 1774.
[50] W. Rieβ, T. A. Beierlein, H. Riel, *Phys. Status Solidi A* **2004**, *201*, 1360.
[51] H. Riel, S. Karg, T. Beierlein, B. Ruhstaller, W. Rieβ, *Appl. Phys. Lett.* **2003**, *82*, 466.
[52] H. Riel, S. Karg, T. Beierlein, W. Rieβ, K. Neyts, *J. Appl. Phys.* **2003**, *94*, 5290.
[53] C. J. Lee, R. B. Pode, D. G. Moon, J. L. Han, N. H. Park, S. H. Baik, S. S. Ju, *Phys. Status Solidi A* **2004**, *201*, 1022.
[54] R. B. Pode, C. J. Lee, D. G. Moon, J. I. Han, *Appl. Phys. Lett.* **2004**, *84*, 4614.
[55] D. G. Moon, R. B. Pode, C. J. Lee, J. I. Han, *Appl. Phys. Lett.* **2004**, *85*, 4771.
[56] S. F. Hsu, C. C. Lee, A. T. Hu, C. H. Chen, *Curr. Appl. Phys.* **2004**, *4*, 663.
[57] D. G. Moon, R. B. Pode, C. J. Lee, J. I. Han, *Mater. Sci. Eng., B* **2005**, *121*, 232.
[58] Y. Q. Li, L. W. Tan, X. T. Hao, K. S. Ong, F. R. Zhu, L. S. Hung, *Appl. Phys. Lett.* **2005**, *86*, 153508.
[59] S. F. Hsu, C. C. Lee, S. W. Hwang, C. H. Chen, *Appl. Phys. Lett.* **2005**, *86*, 253508.
[60] J. Y. Lee, *Appl. Phys. Lett.* **2006**, *88*, 73512.
[61] B. D. Chin, *J. Phys. D: Appl. Phys.* **2007**, *40*, 5541.
[62] Z. Y. Xie, Y. Q. Li, F. L. Wong, L. S. Hung, *Mat. Sci. Eng., B* **2004**, *106*, 219.
[63] Z. Y. Xie, L. S. Hung, F. R. Zhu, *Chem. Phys. Lett.* **2003**, *381*, 691.
[64] G. G. Qin, A. G. Xu, G. L. Ma, G. Z. Ran, Y. P. Qiao, B. R. Zhang, W. X. Chen, S. K. Wu, *Appl. Phys. Lett.* **2004**, *85*, 5406.
[65] S. F. Chen, W. F. Xie, W. Huang, S. Y. Liu, *Opt. Express* **2008**, *16*, 8868.
[66] S. F. Chen, W. F. Xie, Y. L. Meng, P. Chen, Y. Zhao, S. Y. Liu, *J. Appl. Phys.* **2008**, *103*, 54506.
[67] S. Chen, X. Li, W. Huang, *Org. Electron.* **2008**, *9*, 1112.
[68] J. H. Lee, D. S. Leem, J. J. Kim, *Org. Electron.* **2008**, *9*, 805.
[69] G. L. Ma, G. Z. Ran, A. G. Xu, Y. P. Qiao, W. Q. Zhao, B. R. Zhang, S. K. Wu, G. G. Qin, *Appl. Surf. Sci.* **2006**, *252*, 3580.
[70] G. L. Ma, G. Z. Ran, A. G. Xu, Y. H. Xu, Y. P. Qiao, W. X. Chen, L. Dai, G. G. Qin, *Appl. Phys. Lett.* **2005**, *87*, 81106.
[71] S. Han, X. Feng, Z. H. Lu, D. Johnson, R. Wood, *Appl. Phys. Lett.* **2003**, *82*, 2715.
[72] B. Y. Jung, N. Y. Kim, C. Lee, C. K. Hwangbo, C. Seoul, *Appl. Optics* **2002**, *41*, 3312.
[73] Y. C. Lin, W. Q. Lu, in *Optics Theory of Thin Films*, National Defence and Industry Press, Beijing, China **1990**, 63.
[74] A. Dodabalapur, L. J. Rothberg, R. H. Jordan, T. M. Miller, R. E. Slusher, J. M. Phillips, *J. Appl. Phys.* **1996**, *80*, 6954.
[75] D. G. Deppe, C. Lei, C. C. Lin, D. L. Huffaker, *J. Mod. Optics* **1994**, *41*, 325.
[76] T. Shiga, H. Fujikawa, Y. Taga, *J. Appl. Phys.* **2003**, *93*, 19.
[77] C. L. Lin, H. W. Lin, C. C. Wu, *Appl. Phys. Lett.* **2005**, *87*, 21101.
[78] S. K. So, W. K. Choi, L. M. Leung, K. Neyts, *Appl. Phys. Lett.* **1999**, *74*, 1939.
[79] N. E. J. Hunt, E. F. Schubert, R. F. Kopf, D. L. Sivco, A. Y. Cho, G. J. Zydzik, *Appl. Phys. Lett.* **1999**, *63*, 2600.
[80] E. F. Schubert, N. E. J. Hunt, M. Micovic, R. J. Malik, D. L. Sivco, A. Y. Cho, G. J. Zydzik, *Science* **1994**, *265*, 943.
[81] A. M. Vredenberg, N. E. J. Hunt, E. F. Schubert, D. C. Jacobson, J. M. Poate, G. J. Zydzik, *Phys. Rev. Lett.* **1993**, *71*, 517.
[82] R. H. Jordan, L. J. Rothberg, A. Dodabalapur, R. E. Slusher, *Appl. Phys. Lett.* **1996**, *69*, 1997.
[83] E. F. Schubert, N. E. J. Hunt, R. J. Malik, M. Micovic, D. L. Miller, *J. Lightwave Technol.* **1996**, *14*, 1721.
[84] C. J. Lee, R. B. Pode, J. I. Han, D. G. Moon, *Appl. Phys. Lett.* **2006**, *89*, 123501.
[85] S. F. Chen, Z. Y. Zhao, Z. H. Jie, W. F. Xie, Y. Zhao, R. L. Song, C. N. Li, B. F. Quan, S. Y. Liu, *J. Phys. D: Appl. Phys.* **2006**, *39*, 3738.

[86] W. F. Xie, Z. J. Wu, S. Y. Liu, S. T. Lee, *J. Phys. D: Appl. Phys.* **2003**, *36*, 2331.
[87] S. F. Chen, L. H. Xie, C. Y. Chen, J. Xie, W. Huang, S. Y. Liu, *Chinese patent CN200910026491.6,* **2009**.
[88] J. H. Hou, J. Wu, Z. Y. Xie, L. X. Wang, *Org. Electron.* **2008**, *9*, 959.
[89] Y. L. Meng, W. F. Xie, G. H. Xie, L. T. Zhang, Y. Zhao, J. Y. Hou, S. Y. Liu, *Opt. Express* **2009**, *17*, 5364.
[90] R. J. Holmes, B. W. D'Andrade, S. R. Forrest, X. Ren, J. Li, M. E. Thompson, *Appl. Phys. Lett.* **2003**, *83*, 3818.
[91] Y. Kawamura, S. Yanagida, S. R. Forrest, *J. Appl. Phys.* **2002**, *92*, 87.
[92] J. Kido, H. Shionoya, K. Nagai, *Appl. Phys. Lett.* **1995**, *67*, 2281.
[93] J. Kido, K. Hongawa, K. Okuyama, K. Nagai, *Appl. Phys. Lett.* **1994**, *64*, 815.
[94] S. Tasch, E. J. W. List, O. Ekström, W. Graupner, G. Leising, P. Schlichting, U. Rohr, Y. Geerts, U. Scherf, K. Müllen, *Appl. Phys. Lett.* **1997**, *71*, 2883.
[95] M. Granström, O. Inganäs, *Appl. Phys. Lett.* **1996**, *68*, 147.
[96] G. Cheng, F. Li, Y. Duan, J. Feng, S. Y. Liu, S. Qiu, D. Lin, Y. G. Ma, S. T. Lee, *Appl. Phys. Lett.* **2003**, *82*, 4224.
[97] B. W. D'Andrade, M. A. Baldo, C. Adachi, J. Brooks, M. E. Thompson, S. R. Forrest, *Appl. Phys. Lett.* **2001**, *79*, 1045.
[98] M. Berggren, G. Gustafsson, O. Inganäs, M. R. Andersson, T. Hjertberg, O. Wennerström, *J. Appl. Phys.* **1994**, *76*, 7530.
[99] J. Feng, F. Li, W. B. Gao, S. Y. Liu, Y. Liu, Y. Wang, *Appl. Phys. Lett.* **2001**, *78*, 3947.
[100] B. W. D'Andrade, J. Brooks, V. Adamovich, M. E. Thompson, S. R. Forrest, *Adv. Mater.* **2002**, *14*, 1032.
[101] V. Adamovich, J. Brooks, A. Tamayo, A. M. Alexander, P. I. Djurovich, B. W. D'Andrade, C. Adachi, S. R. Forrest, M. E. Thompson, *New J. Chem.* **2002**, *26*, 1171.
[102] J. Brooks, Y. Babayan, S. Lamansky, P. I. Djurovich, I. Tsyba, R. Bau, M. E. Thompson, *Inorg. Chem.* **2002**, *41*, 3055.
[103] S. W. Lai, M. Chan, T. C. Cheung, S. M. Peng, C. M. Che, *Inorg. Chem.* **1999**, *38*, 4046.
[104] A. Dodabalapur, L. J. Rothberg, T. M. Miller, *Appl. Phys. Lett.* **1994**, *65*, 2308.
[105] A. Dodabalapur, L. J. Rothberg, T. M. Miller, *Electron. Lett.* **1994**, *30*, 1000.
[106] J. J. Shiang, T. J. Faircloth, A. R. Duggal, *J. Appl. Phys.* **2004**, *95*, 2889.
[107] G. Parthasarathy, G. Gu, S. R. Forrest, *Adv. Mater.* **1999**, *11*, 907.
[108] T. Feng, T. A. Au, E. S. Ramakrislman, R. Campos, W. E. Howard, *Proc. SPIE* **2001**, *4105*, 30.
[109] M.-T. Lee, M.-R. Tseng, *Curr. Appl. Phys.* **2008**, *8*, 616.
[110] http://www.engadget.com/2007/01/08/sonys-1--000-000--1-contrast-ratio-27-inch-oled-hdtv/.
[111] http://www.emagin.com/products/index.php.